RSC Advances

ROYAL SOCIETY OF CHEMISTRY

www.rsc.org/advances

RSC Advances

RSCPublishing

ARTICLE

One-step green synthesis of arginine-capped iron oxide/reduced graphene oxide nanocomposite and its use for acid dye removal

Cite this: DOI: 10.1039/xoxxoooooox

Received ooth April 2014,
Accepted ooth oooo 2014

DOI: 10.1039/xoxxoooooox

www.rsc.org/

Tzu-Yang Lin and Dong-Hwang Chen*

An arginine-capped nanocomposite of iron oxide nanoparticles and reduced graphene oxide (iron oxide/rGO) has been synthesized as a magnetic nano-adsorbent for the removal of acid dyes via a facile one-step green route with L-arginine as the reducing agent and capping agent. The resulting iron oxide/rGO nanocomposite had an isoelectric point of about pH 4 and was magnetically recoverable owing to the L-arginine capping and iron oxide nanoparticles decoration. Also, it was quite efficient for the adsorption of acid dyes due to the electrostatic interaction and the van der Waals force or π−π interaction between the acid dyes and the arginine-capped iron oxide/rGO nanocomposite. The adsorption capacity increased with the increase of rGO content and was much higher than those of iron oxide nanoparticles and GO. Furthermore, although the adsorption capacity decreased with the increase of pH, it still remained significant adsorption ability in the examined pH range of 2–6. Moreover, the adsorption for both acid dyes obeyed the Langmuir isotherms and the adsorption capacity increased with the increase of temperature, revealing a diffusion controlled mechanism. In addition, the adsorption process obeyed the pseudo second-order kinetic model. Also, both acid dyes could be desorbed by NaOH solution and the iron oxide/rGO nanocomposite exhibited good reusability.

1. Introduction

Industries based on textiles, paper, leather, food, and cosmetics use very large amount of dyes, and the waste from these industries is a major environmental concern.[1] Therefore, the removal of various dyes to alleviate effluent pollution from industries is an important area of basic and applied research. Until now, adsorption is still considered as one of the most convenient and efficient methods to remove dyes from aqueous solutions. In general, to ensure a sufficiently large surface area for adsorption, adsorbents are usually highly porous particles such as activated carbon,[2] aerogels,[3] zeolites[4] and clays[5]. However, the existence of intraparticle diffusion may lead to the decreases in the adsorption rate and available capacity, particularly for macromolecules.[6–8] Therefore, to develop an adsorbent with large surface area and small diffusion resistance still remains demanded in practical application.

Graphene is a planar monolayer of carbon atoms arranged into a 2-dimensional honeycomb lattice with sp^2 hybridized. This unique structure endows it and its derivatives such as graphene oxide (GO) and reduced graphene oxide (rGO) with various superior properties, including high specific surface area (~2630 m^2/g), partially filled π-orbitals above and below the plane of the sheet, unique optical property, and good electrical, thermal and mechanical properties.[9–15] Because of the high specific surface area, 2-dimensional nano-sheet structure, and abundant oxygen-containing functional groups, graphene and its derivatives have become promising adsorbents with high adsorption capacity and low diffusion resistance. Recently, it has been demonstrated that the graphene-based adsorbents are effective for the removal of heavy metals (Pb^{2+}, Cd^{2+}, Co^{2+}, etc.)[16,17] and dyes (methyl orange, methyl violet, rhodamine B, methylene blue and Bisphenol A, etc.)[18–22] via the strong π−π stacking, anion−cation interaction or hydrogen bonding. By the surface modification or nanoparticles decoration, they could be further used for the adsorption of biomolecules,[23] inorganic toxic compounds As(III) and As(V),[24] and more heavy metals and organic pollutants.[25–28] It was mentionable that the unmodified GO was negatively charged owing to the oxygen-containing functional groups. So, its ability for the adsorption of acid dyes was expected to be weak and further surface modification was needed to overcome this problem. Furthermore, it was also noted that some works have been done for the decoration of iron oxide nanoparticles on the surface of graphene sheets, which made the nanocomposites become magnetically recoverable.[29–36] Accordingly, for the efficient adsorption removal of acid dyes from aqueous solutions and the easy recovery of adsorbents, it was desired to fabricate a graphene-based adsorbent with iron oxide nanoparticles decoration for magnetic recovery and surface modification for acid dye adsorption in this work.

Department of Chemical Engineering, National Cheng Kung University, Tainan, Taiwan 701, Republic of China. E-mail: chendh@mail.ncku.edu.tw

On the other hand, to reduce or eliminate the use of substances hazardous to human health and the environment, the development of green chemical processes and products is becoming more and more important in the past decade.[37,38] L-arginine, one of the common natural amino acids, has been used successfully for the green synthesis of some metal and metal oxide nanoparticles.[39–41] It was suggested that L-arginine not only played a role of reducing agent but also acted as a capping agent.[41] Recently, we also successfully prepared the Ag/iron oxide nanocomposite as a magnetically recoverable catalyst using L-arginine as the reducing agent.[42] Because the surface capping with L-arginine might introduce amino acid groups and make the surface of GO become positively charged in appropriate pH range, in this work we attempted to develop a facile and environmentally friendly one-step green method to produce the iron oxide/reduced graphene oxide (rGO) nanocomposite using L-arginine as the reducing agent and capping agent simultaneously. The resulting nanocomposite was further demonstrated to be efficient for the adsorption of acid dyes using crocein orange G (AO12) and acid green 25 (AG25) as model compounds.

2. Materials and methods

2.1. Materials

Graphite powder (99.9%) was obtained from Bay Carbon. Potassium manganite (VII) and sodium nitrate were purchased from J. T. Baker. Sulfuric acid was supplied by Panreac. Hydrogen peroxide was a product of Showa. Sulfuric acid was obtained from Merck. L-arginine and iron (II) chloride tetrahydrate were supplied by Sigma–Aldrich. Crocein orange G and acid green 25 were purchased from Fluka and Aldrich, respectively. All chemicals were of guaranteed or analytical grade reagents commercially available and used without further purification. The water used throughout this work was the reagent grade water produced by a Milli-Q SP ultra-pure-water purification system of Nihon Millipore Ltd., Tokyo.

2.2. Synthesis of graphene oxide

GO was prepared from purified natural graphite via the modified Hummers method.[43] At first, graphite powder (1.5 g) and $NaNO_3$ (0.75 g) were added to the concentrated H_2SO_4 (18 M, 37 mL) in an ice-bath. Secondly, $KMnO_4$ (4.5 g) was added gradually under stirring. The mixture was stirred at 35°C for 24 h, and then at 98°C for 15 min after the slow addition of deionized water (70 mL). Next, the suspension was further diluted to 110 mL and stirred for another 30 min. Finally, the reaction was terminated by adding H_2O_2 (3.7 mL, 35 wt %) under stirring at room temperature, followed by washing with deionized water several times.

2.3. Synthesis of iron oxide/rGO nanocomposite

Iron oxide/rGO nanocomposite was synthesized according to our previous work on the synthesis of Ag/iron oxide nanocomposite.[42] Typically, for the preparation of iron oxide/rGO nanocomposite with a Fe/GO weight ratio of 1/1, 10 mg of GO was dispersed in L-arginine solution (15 mL) with ultrasonication for 30 min at first and then stirred in a water bath at 70°C. Secondly, about 35 mg of $FeCl_2{\cdot}4H_2O$ was added under continuous stirring. Finally, the reaction was conducted at 70°C for 20 h to yield a homogeneous black solution. The product was recovered magnetically by a magnet, washed with ethanol for three times, and then dried in an oven at 60°C. For the preparation of iron oxide/rGO nanocomposites with the Fe/GO weight ratios of 1/2 or 2/1, different amount of $FeCl_2{\cdot}4H_2O$ was added under a fixed GO amount according to the above procedures. Unless otherwise specified, the iron oxide/rGO nanocomposite with a Fe/GO weight ratio of 1/1 was used for the material characterization and adsorption/desorption measurements throughout this work. In addition, for comparison, rGO and iron oxide nanoparticles were also prepared according to the above procedures in the absence of $FeCl_2$ and GO, respectively.

2.4. Characterization

The TEM and high-resolution TEM (HRTEM) images, composition, and selected area electron diffraction (SAED) pattern were obtained by a JEOL Model JEM-2100F electron microscope at 200 kV. The crystalline structures were characterized by X-ray diffraction (XRD) analysis on a Shimadzu model RX-III X-ray diffractometer at 40 kV and 30 mA with CuKα radiation (λ = 0.1542 nm). Raman scattering was performed on a Thermo Fisher Scientific DXR Raman Microscopy using a 532 nm laser source. Fourier Transform Infrared (FTIR) spectra were recorded on a Varian FTS-1000 FTIR spectrometer. The X-ray photoelectron spectroscopy (XPS) measurement was performed on a KRATOS AXIS Ultra DLD photoelectron spectrophotometer with an achromatic Mg/Al X-ray source at 450W. The zeta potentials were measured on a Malvern Zetasizer Nano Z. The pH dependences of zeta potentials for GO, rGO, and iron oxide/rGO nanocomposite (0.25 mg/mL) were measured in the aqueous solutions at different pH values, adjusted by NaOH and HCl. Magnetic measurement was performed on a superconducting quantum interference device (SQUID) magnetometer (MPMS7, Quantum Design). The BET surface area was determined by using the gas sorption technique with a Micromeritics ASAP 2020.

2.5. Adsorption/desorption of acid dyes

For the adsorption of acid dyes, 2 mg of GO, iron oxide, or iron oxide/rGO nanocomposite was added to 10 mL of the aqueous solution containing AO12 or AG25 at the desired temperature and pH for 2–3 h to ensure the adsorption equilibrium. The solution pH was adjusted by the addition of NaOH and HCl solutions. The concentrations of acid dyes were determined from the absorbances at 482 and 640 nm for AO12 and AG25, respectively, by a JASCO model V-570 UV/VIS/NIR spectrophotometer. The adsorption kinetics was studied in aqueous solution at pH 2, 30°C, and an initial acid dye concentration of 30 mg/L. The concentrations of acid dyes at various time intervals were determined spectrophotometrically by using a magnet to hold the magnetic nanocomposite on the wall of vessel. The desorption of acid dyes was studied by using NaOH solutions (10 mL) at different concentrations. The samples used for the desorption experiments were obtained from the adsorption experiments at pH 2, 30ºC, and the initial acid dye concentration of 30 (AO12) or 50 (AG25) mg/L. The desorption time was 2–3 h. To examine the reusability, for each cycle, the adsorption was conducted at pH 2, 30ºC, and the initial acid dye concentration of 30 (AO12) or 50 (AG25) mg/L while the desorption was carried out using 0.1 M NaOH (10 mL) for 1 h and repeated 3 times.

3. Results and discussion

3.1. Basic properties of iron oxide/rGO nanocomposite

Fig. 1a shows the typical TEM image of iron oxide/rGO nanocomposite. It was found that a lot of iron oxide nanoparticles were decorated on the surface of rGO. In spite of

high coverage, No significant agglomeration was observed. From the magnified image as indicated in Fig. 1b, the decorated iron oxide nanoparticles could be observed more clearly and their mean diameter could be estimated to be 7.82±2.22 nm from the inset. Furthermore, the HRTEM image as shown in Fig. 1c revealed the lattice spacings of 2.54 and 1.47 Å. They related to the (311) and (440) planes of Fe_3O_4. Also, from the corresponding electron diffraction pattern as shown in Fig. 1d, three fringe patterns with plane distances of 0.25, 0.15, 0.32 nm were observed. They related to the (311) and (440) planes of Fe_3O_4 and the (020) plane of FeOOH, respectively. These results revealed the successful decoration of iron oxide nanoparticles on the surface of rGO. By EDX analysis as indicated in Fig. 2, the presence of Fe element confirmed the deposition of iron oxide nanoparticles. The weight percentage of Fe element in the product was about 38.7%. In addition, it was noted that N element (about 10.2 wt%) was also present. This might be due to the L-arginine and implied that L-arginine has been capped on the surface of iron oxide/rGO nanocomposite.

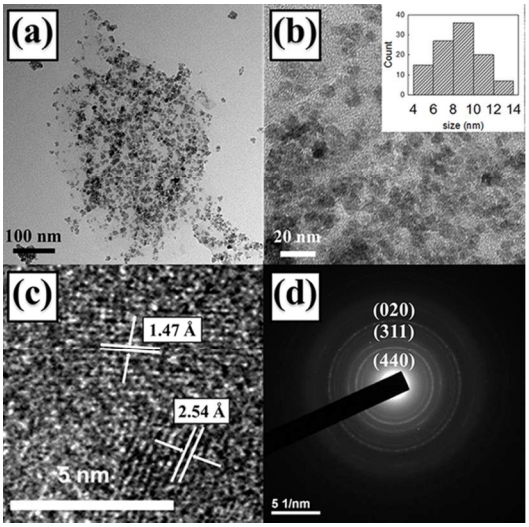

Fig. 1 Typical TEM (a,b) images, HRTEM image (c), and electron diffraction pattern of iron oxide/rGO nanocomposite. The inset in (b) is the particle size distribution.

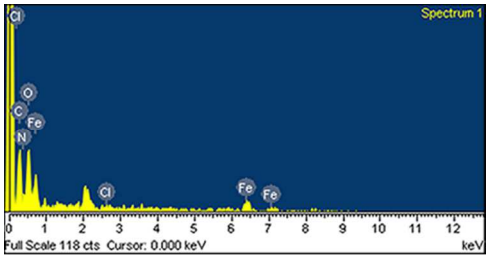

Fig. 2 EDX spectrum of iron oxide/rGO nanocomposite.

Fig. 3 shows the XRD patterns of GO, rGO, and the iron oxide/rGO nanocomposite obtained after different reaction times. The characteristic peaks of GO and rGO were observed at about 2θ = 10.5° and 23.0°, respectively, confirming GO has been reduced to rGO successfully by L-arginine. For iron oxide/rGO nanocomposite, three main characteristic peaks were observed at 2θ = 14.0, 35.5, and 62.4° after reaction for 20 h. They were corresponding to the (020) plane of FeOOH and the (311) and (440) planes of Fe_3O_4. This confirmed that the iron oxide nanoparticles decorated on the surface of rGO were the mixture of Fe_3O_4 and FeOOH. In addition, it was mentionable that the iron oxide/rGO nanocomposite could be magnetically recovered easily even the reaction time was only 5 h. So, the more significant characteristic peaks of iron oxide obtained at longer reaction times should be due to the improvement of crystallinity.

The Raman spectra of GO, rGO, and iron oxide/rGO nanocomposite were shown in Fig. 4. Two prominent peaks corresponding to the G and D bands were observed clearly. The intensity ratios of D band to G band (I_D/I_G) for GO, rGO, and iron oxide/rGO nanocomposite were 0.77, 1.07, and 1.15, respectively. It is known that the G band is usually due to the E_{2g} phonon of C sp^2 atoms while the D band originates from a breathing κ-point phonon with A_{1g} symmetry and relates to local defects and disorders.[44–46] Furthermore, higher I_D/I_G ratio means the smaller size of sp^2 domains.[47] The conjugated graphene network (sp^2 carbon) will be re-established after chemical reduction of GO and the size of the re-established graphene network is usually smaller than the original graphite layer, leading to the increase of I_D/I_G ratio.[48,49] Thus, the larger I_D/I_G ratios of rGO and iron oxide/rGO nanocomposite than that of GO demonstrated that GO was also reduced to rGO simultaneously by L-arginine. In addition, the I_D/I_G ratio of iron oxide/rGO nanocomposite was slightly larger than that of rGO. This might be due to the increase in the number of defects after the deposition of iron oxide nanoparticles on rGO.

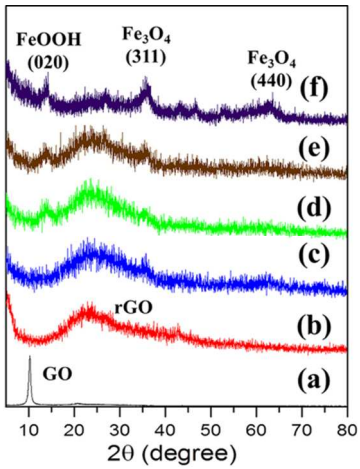

Fig. 3 XRD patterns of GO (a), rGO (b), and the iron oxide/rGO nanocomposite obtained after reaction for 5 (c), 10 (d), 15 (e), and 20 (f) h.

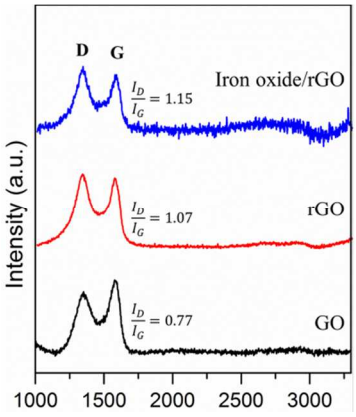

Fig. 4 Raman spectra of GO, rGO, and iron oxide/rGO nanocomposite.

Fig. 5 shows the FTIR spectra of L-arginine, GO, rGO, and iron oxide/rGO nanocomposite. For GO, the characteristic peaks at 1734 and 1623 cm^{-1} were due to the C=O stretching of the carbonyl and carboxylic groups, respectively, on GO. The broad peak at 1420 cm^{-1} could be assigned to the -COOH combination band owing to the C-O stretching and O-H deformation. The peak around 1009 cm^{-1} was resulted from the C–O stretching vibration. For L-arginine, two characteristic peaks due to the C=O stretching of carboxylic groups and the N–H bending vibration of imine group could be observed clearly at 1630 and 1570 cm^{-1}, respectively. When GO was reduced to rGO by L-arginine, the characteristic peaks of GO around 1420 and 1009 cm^{-1} became weaker for both rGO and the iron oxide/rGO nanocomposite. This revealed GO was partially reduced. Furthermore, it was found that the characteristic peak around 1623 cm^{-1} was enhanced significantly and combined the characteristic peak at 1734 cm^{-1} into a larger one. Also, a characteristic peak appeared at 1570 cm^{-1}, which should be resulted from the N–H bending vibration of imine group. The iron oxide/rGO nanocomposite also exhibited a similar spectrum as rGO did in the wavenumber range of 1500 to 1700 cm^{-1}. These evidences revealed that L-arginine has been capped on the surfaces of rGO and iron oxide/rGO nanocomposite. In addition, the spectrum of iron oxide/rGO nanocomposite also showed a characteristic peak at 572 cm^{-1}. It was due to the stretching vibration of Fe–O and demonstrated the deposition of iron oxide on rGO.

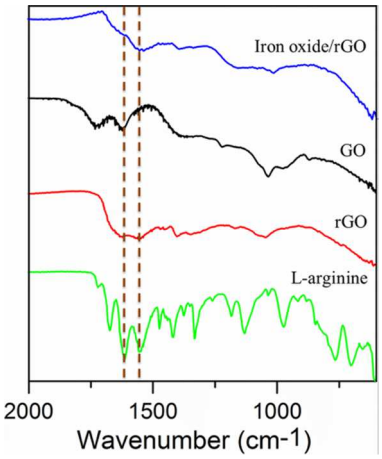

Fig. 5 FTIR spectra of L-arginine, GO, rGO, and iron oxide/rGO nanocomposite.

The C1s XPS spectrum of GO as shown in Fig. 6a revealed the characteristic peaks of C-C, C=C (at 284.8 eV), C-O-H, C-O-C (at 286.9 eV), and C=O (at 288.05 eV). They could be attributed to the presence of epoxide, hydroxyl, and carboxyl groups.[48,49] For iron oxide/rGO nanocomposite, the full survey XPS spectrum (Fig. 6b) not only indicates the peaks of C1s and O1s but also those of N1s and Fe2p. They could be attributed to the arginine capping and the deposition of iron oxide on rGO. The Fe2p XPS spectrum (Fig. 6c) shows the binding energy peaks of $Fe2p_{3/2}$ and $Fe2p_{1/2}$ at 710.5 and 724.4 eV, respectively. The disappearance of the charge transfer satellite of Fe $2p_{3/2}$ around 720 eV revealed the formation of a mixed oxide of Fe(II) and Fe(III) such as Fe_3O_4.[29] The high-resolution Fe $2p_{3/2}$ XPS spectrum as shown in the inset of Fig. 6c further revealed the presence of different iron oxides. The peaks at 710.4 and 713.6 eV related to $Fe_3O_4(Fe^{2+})$ and $Fe_3O_4(Fe^{3+})$, while the peak at 712.1 eV was due to FeOOH and the peak at 711.2 eV covered both of Fe_3O_4 and FeOOH.[50] Fig. 6d shows the C1s XPS spectrum of iron oxide/rGO nanocomposite. As compared to that of GO (Fig. 6a), the peak intensity of C1s which related to oxygenated functional groups (C-O-H, C-O-C, and C=O) showed a significant decrease, confirming that most of the epoxide, hydroxyl, and carboxyl functional groups were removed and GO has been reduced.[48,49] It was noted that two new characteristic peaks of C-N and O-C=O were observed. They might be due to the L-arginine capped on the surface of iron oxide/rGO nanocomposite. All the above results were consistent with the XRD and FTIR analyses.

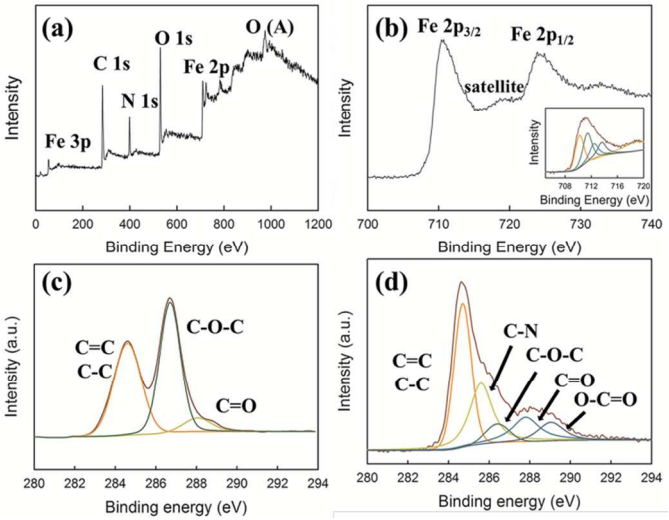

Fig. 6 C1s XPS spectrum of GO (a) and the full survey (b), Fe 2p (c) and C1s (d) XPS spectra of iron oxide/rGO nanocomposite.

Fig. 7 shows the pH dependences of zeta potentials for GO, rGO, and iron oxide/rGO nanocomposite. It was obvious that the isoelectric points of rGO and iron oxide/rGO nanocomposite were about 5 and 4, respectively. According to the study of Lai et al.,[40] the isoelectric point of arginine-capped Fe_3O_4 nanoparticles was about 5.61, which was the average of the pK_a of carboxylic group and the pK_b of amine group. In this work, the isoelectric points of rGO and iron oxide/rGO nanocomposite were much higher than that of GO and only slightly lower than that of arginine-capped Fe_3O_4 nanoparticles. This provided another evidence to demonstrate that L-arginine has been capped on the surface of rGO and iron oxide/rGO nanocomposite.

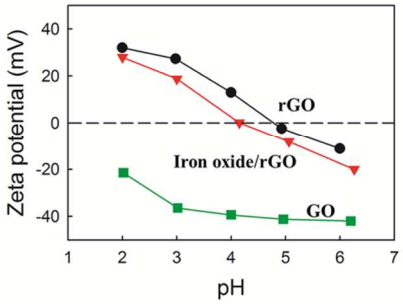

Fig. 7 Zeta potential of GO, rGO and iron oxide/rGO nanocomposite.

Fig. 8 shows the plot of magnetization versus magnetic field (M-H loop) at 25ºC for iron oxide/rGO nanocomposite. The weak hysteresis revealed that they were nearly

superparamagnetic. From the M-H loop and its enlargement near the origin as shown in the upper-left inset of Fig. 8, the saturation magnetization (M_s), remanent magnetization (M_r), coercivity (H_c), and squareness (S_r=M_r/M_s) could be determined to be 16.97 emu/g, 0.65 emu/g, 54.62 Oe, and 0.038, respectively. The lower-right inset of Fig. 8 shows the photographs for the aqueous solutions of AO12 in the absence and presence of iron oxide/rGO nanocomposite with a magnet on the outer wall of the vessel. It was obvious that the iron oxide/rGO nanocomposite could adsorb AO12 effectively and be held on the inner wall completely. This demonstrated that the iron oxide/rGO nanocomposite could be used as a magnetically recoverable adsorbent of acid dyes.

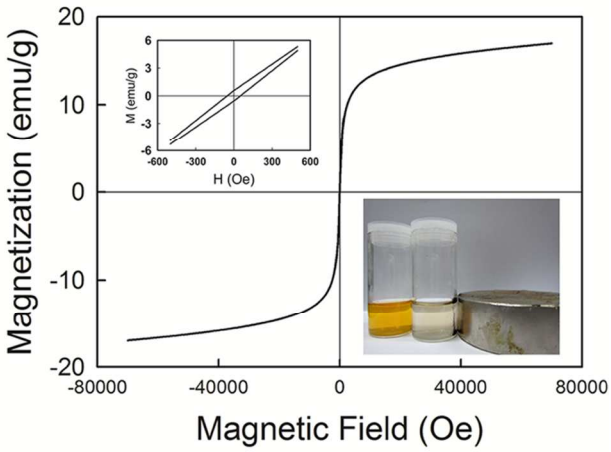

Fig. 8 Magnetization vs. magnetic field of iron oxide/rGO nanocomposite. The upper-left inset is the enlargement near the origin. The lower-right inset is the photographs for the aqueous solutions of AO12 in the absence (left) and presence (right) of iron oxide/rGO nanocomposite with a magnet on the outer wall of the vessel.

The BET surface area of iron oxide/rGO nanocomposite was determined to be about 104 m^2/g. Such a value was comparable to some reported works.[29,35,36] In addition to the decoration of iron oxide, the significantly lower specific surface area than the theoretical value of graphene (about 2630 m^2/g) was mainly due to the agglomeration of nanocomposite because the sample for surface area analysis had to be dried. In fact, in the aqueous solution, the agglomeration was insignificant and a higher specific surface area was expected.

3.2. Adsorption property of iron oxide/rGO nanocomposite

Fig. 9 shows the adsorption capacity of GO, iron oxide, and iron oxide/rGO nanopcomposites with different Fe/GO weight ratios at 30°C and various pH values for AO12 and AG25. The initial concentrations of AO12 and AG25 were 30 and 50 mg/L, respectively. It was obvious that the iron oxide/rGO nanocomposites exhibited significantly higher adsorption capacity and the adsorption capacity increased with the increase of rGO content due to the large specific surface area. It was mentionable that the adsorption capacities of rGO and iron oxide/rGO nanocomposite with much higher rGO content were not examined because their excellent dispersion property made them difficult to be recovered from the aqueous solutions. In addition, the adsorption capacity decreased with the increase of pH value. However, it was noted that, even at the pH above 4, the iron oxide/rGO nanocomposites still possessed high adsorption capacity for AO12 and AG25. When pH was below the isoelectric point, the adsorption might be mainly due to the electrostatic interaction between acid dyes and the arginine-capped iron oxide/rGO nanocomposite. When pH was above the isoelectric point, the adsorption might be resulted from the van der Waals force or π–π interactions.

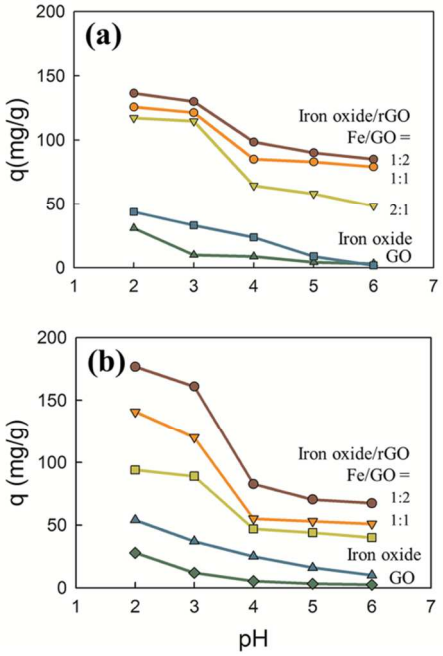

Fig. 9 Adsorption capacity of GO, iron oxide, and iron oxide/rGO nanopcomposites with different ratios of iron oxide to rGO at 30°C and various pH values for AO12 (a) and AG25 (b).

Fig. 10 shows the adsorption isotherms of iron oxide/rGO nanopcomposite at pH 2 and different temperatures (20, 30, and 40°C) for AO12 (initial concentration 10-50 mg/L) and AG25 (initial concentration 10-50 mg/L). The adsorption capacity increased with increasing the temperature. As indicated in the insets of Fig. 10, the linear dependences of C_e/q on C_e at pH 2 and different temperatures revealed that the adsorption followed Langmuir isotherm for both AO12 and AG25. The corresponding maximum capacities (q_m) and Langmuir adsorption constants (K_L) were listed in Table 1. In addition, it was obvious that both q_m and K_L values for AO12 and AG25 increased with the increase in the temperature. The corresponding Gibbs energy (ΔG°), enthalpy (ΔH°), and entropy (ΔS°) could be calculated according to the following equations:[51]

$$\Delta G^\circ = -RT\ln K_L \quad (1)$$

$$\ln K_L = -\frac{\Delta H^\circ}{RT} + \frac{\Delta S^\circ}{R} \quad (2)$$

where R and T are gas constant and temperatures, respectively. It was found the ΔG°, ΔH°, and ΔS° values at 30°C were -0.21 kJ/mol, 15.98 kJ/mol, 62.52 J/K-mol for AO12 and -0.34 kJ/mol, 25.12 kJ/mol, 86.52 J/K-mol for AG25, respectively. The endothermic property implied that the adsorption was diffusion controlled.[51]

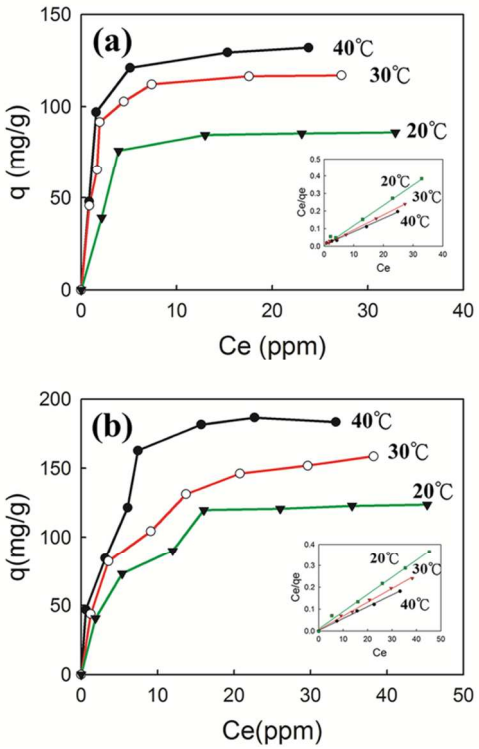

Fig. 10 Adsorption isotherms of iron oxide/rGO nanopcomposite at pH 2 and different temperatures for AO12 (a) and AG25 (b). The insets indicate the dependences of C_e/q on C_e for the adsorption of AO12 (a) and AG25 (b) by iron oxide/rGO nanopcomposite at pH 2 and different temperatures. q_e is the equilibrium adsorption capacity and C_e is the equilibrium concentration in solution.

Table 1 q_m and K_L values for the adsorption of AO12 and AG25 by iron oxide/rGO nanocomposite at different temperatures

	AO12		AG25	
Temp(°C)	q_m (mg/g)	K_L (L/g)	q_m (mg/g)	K_L (L/g)
20	99.0	0.689	126.6	0.849
30	117.6	1.089	158.7	1.145
40	131.6	1.490	185.2	1.688

To further examine the adsorption kinetics, the pseudo first-order and pseudo second-order kinetic models as shown below were tested to find out the appropriate adsorption rate expression:[36]

$$\ln(q_e - q_t) = \ln q_e - k_1 t \quad (3)$$

$$\frac{t}{q_t} = \frac{1}{k_2 q_e^2} + \left(\frac{1}{q_e}\right)t \quad (4)$$

where q_t and q_e are the amounts of acid dye adsorbed at the time t and at equilibrium (mg/g), k_1 is the rate constant of the pseudo first-order adsorption process (min^{-1}), and k_2 is the pseudo second-order rate constant (g/mg-min). Fig. 11 shows the adsorption kinetics of AO12 and Ag25 and the corresponding plots for the pseudo first-order and pseudo second-order kinetic models in the aqueous solutions at pH 2, 30°C, and an initial concentration of 30 mg/L. It was found, for AO12, k_1 and k_2 were 0.04 min^{-1} and 1.0×10^{-4} g/mg-min with R-square values of 0.90 and 0.99, respectively. For AG25, k_1 and k_2 were 0.024 min^{-1} and 2.3×10^{-4} g/mg-min with R-square values of 0.97 and 0.99, respectively. Thus, the pseudo second-order kinetic model might describe the adsorption kinetics better than the pseudo first-order kinetic model.

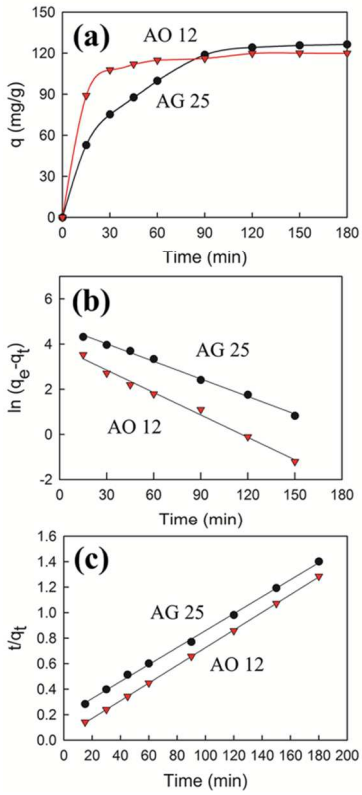

Fig. 11 Adsorption kinetics (a) and the corresponding plots for the pseudo first-order (b) and pseudo second-order (c) kinetic models.

Fig. 12a shows the desorption of AO12 and AG25 by the NaOH solutions at different concentrations. It was found that NaOH solution could be efficiently used for the desorption of both acid dyes. For AG25, about 70% desorption could be obtained by 0.01M NaOH solution. For AO12, the desorption was only about 50% at the same NaOH concentration. This was similar to the previous study and could be attributed to their different pH effect. The reusability of iron oxide/rGO nanocomposite for the adsorption/desorption of AO12 and AG25 was indicated in Fig. 12b. It was obvious that the adsorption capacities had no significant decreases for both acid dyes, revealing the iron oxide/rGO nanocomposite had good stability and reusability.

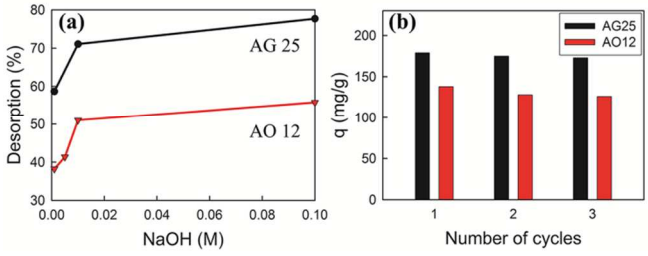

Fig. 12 Desorption of AO12 and AG25 by NaOH solutions (a) and the reusability of iron oxide/rGO nanocomposite (b).

Conclusions

The iron oxide/rGO nanocomposite has been synthesized successfully via a facile green route using L-arginine as the reducing agent and capping agent. From the analyses of TEM, XRD, EDX, XPS, Raman and FTIR spectra, and zeta potential, it was demonstrated that GO was reduced to rGO and the iron oxide nanoparticles of 7.82±2.22 nm were decorated on the surface of rGO simultaneously. Also, the resulting iron oxide/rGO nanocomposite was magnetically recoverable and capped with L-arginine, leading to a shift of zeta potential to about pH 4. As compared to iron oxide nanoparticles and GO, the iron oxide/rGO nanocomposite exhibited a significantly enhanced adsorption capability for the acid dyes (AO12 and AG25) and the adsorption capacity increased with the increase of rGO content owing to its large specific surface area. Although the adsorption capacity decreased with the increase of pH, this nanocomposite exhibited high adsorption capability in the examined pH range of 2–6 due to the electrostatic interaction and the van der Waals force or π−π interactions between acid dyes and the arginine-capped iron oxide/rGO nanocomposite. Furthermore, the adsorption process followed the Langmuir isotherms and was endothermic due to the diffusion controlled mechanism. Also, the adsorption rate could be expressed by the pseudo second-order kinetic model. Both acid dyes could be desorbed by the use of NaOH solution, and the iron oxide/rGO nanocomposite had good reusability.

Acknowledgements

This work was performed under the auspices of the National Science Council of the Republic of China, under contract number NSC 102-2221-E-006-221-MY3, to which the authors wish to express their thanks.

References

1 M. M. Ayad and A. A. El-Nasr, *J. Phys. Chem. C*, 2010, **114**, 14377–14383.
2 K. K. H. Choy, G. McKay and J. F. Porter, *Resour. Conserv. Recy*., 1999, **27**, 57–71.
3 L. Abramian and H. El-Rassy, *Chem. Eng. J*., 2009, **150**, 403–410.
4 S. Wang, H. Li and L. Xu, *J. Colloid Interface Sci*., 2006, **295**, 71–78.
5 G. Crini, *Bioresour. Technol*., 2006, **97**, 1061–1085.
6 M. H. Liao and D. H. Chen, *J. Mater. Chem*., 2002, **12**, 3654–3659.
7 S. S. Banerjee and D. H. Chen, *J. Hazard. Mater*., 2007, **147**, 792–799.
8 S. H. Huang and D. H. Chen, J. *Hazard. Mater*., 2009, **163**, 174-179.
9 H. Wang, X. Yuan, Y. Wu, H. Huang, X. Peng, G. Zeng, H. Zhong, J. Liang and M. M. Ren, *Adv. Colloid Interface Sci*., 2013, **195–196**, 19–40.
10 R. S. Edwards and K. S. Coleman, *Nanoscale*, 2013, **5**, 38–51.
11 A. A. Balandin, S. Ghosh, W. Z. Bao, I. Calizo, D. Teweldebrhan, F. Miao and C. N. Lau, *Nano Lett*. 2008, **8**, 902–907.
12 A. K. Geim, *Science*, 2009, **324**, 1530–1534.
13 A. K. Geim and K. S. Novoselov, *Nat. Mater*., 2007, **6**, 183–191.
14 K. S. Kim, Y. Zhao, H. Jang, S. Y. Lee, J. M. Kim, K. S. Kim, J. H. Ahn, P. Kim, J. Y. Choi and B. H. Hong, *Nature*, 2009, **457**, 706–710.
15 S. Stankovich, D. A. Dikin, G. H. B. Dommett, K. M. Kohlhaas, E. J. Zimney, E. A. Stach, R. D. Piner, S. T. Nguyen and R.S. Ruoff, *Nature*, 2006, **442**, 282–286.
16 X. Deng, L. Lü, H. Li and F. Luo, *J. Hazard. Mater*., 2010, **183**, 923–930.
17 G. Zhao, J. Li, X. Ren, C. Chen and X. Wang, *Environ. Sci. Technol*., 2011, **45**, 10454–10462.
18 F. Liu, S. Chung, G. Oh and T. S. Seo, *ACS Appl. Mater. Interfaces*, 2012, **4**, 922–927.
19 G. K. Ramesha, A.V. Kumara, H. B. Muralidhara and S. Sampath, *J. Colloid Interface Sci*., 2011, **361**, 270–277.
20 Y. Yu, B. N. Murthy, J. G. Shapter, K. T. Constantopoulos, N. H. Voelcker and A. V. Ellis, *J. Hazard. Mater*., 2013, **260**, 330–338.
21 T. Liu, Y. Li, Q. Du, J. Sun, Y. Jiao, G. Yang, Z. Wang, Y. Xia, W. Zhang, K. Wang, H. Zhu and D. Wu, *Colloid Surface B*, 2012, **90**, 197–203.
22 J. Xu, L. Wang and Y. Zhu, *Langmuir*, 2012, **28**, 8418−8425.
23 G. Cheng, Y. L. Liu, Z. G. Wang, J. L. Zhang, D. H. Sunc and J. Z. Ni, *J. Mater. Chem*., 2012, **22**, 21998–22004.
24 V. Chandra, J. Park, Y. Chun, J. W. Lee, I. C. Hwang and K. S. Kim, *ACS Nano*, 2010, **4**, 3979–3986.
25 L. Liu, C. Li, C. Bao, Q. Jia, P. Xiao, X. Liu and Q. Zhang, *Talanta*, 2012, **93**, 350–357.
26 Y. Chen, L. Chen, H. Bai and L. Li, *J. Mater. Chem*. A 2013, **1**, 1992–2001.
27 Y. Wang, S. Wang, H. Niu, Y. Ma, T. Zeng, Y. Cai and Z. Meng, *J. Chromatogr. A*, 2013, **1283**, 20–26.
28 P. Bhunia, G. Kim, C. Baik and H. Lee, *Chem. Commun.*, 2012, **48**, 9888–9890.
29 W. Fan, W. Gao, C. Zhang, W. W. Tjiu, J. Pan and T. Liu, *J. Mater. Chem.*, 2012, **22**, 25108–25115.
30 G. Xie, P. Xi, H. Liu, F. Chen, L. Huang, Y. Shi, F. Hou, Z. Zeng, C. Shao and J. Wang, *J. Mater. Chem*., 2012, **22**, 1033−1039.
31 N. A. Travlou, G. Z. Kyzas, N. K. Lazaridis and E. A. Deliyanni, *Langmuir*, 2013, **29**, 1657−1668.
32 J. Guoa, R. Wanga, W. W. Tjiu, J. Panb and T. Liua, *J. Hazard. Mater*. 2012, **225−226**, 63−73.
33 S. Zhang, M. Zeng, J. Li, J. Li, J. Xu and X. Wang, *J. Mater. Chem. A*, 2014, **2**, 4391–4397.
34 J. Zhu, S. Wei, H. Gu, S. B. Rapole, Q. Wang, Z. Luo, N. Haldolaarachchige, D. P. Young and Z. Guo, *Environ. Sci. Technol.*, 2012, **46**, 977−985.
35 Z. Geng, Y. Lin, X. Yu, Q. Shen, L. Ma, Z. Li, N. Pan and X. Wang, *J. Mater. Chem.*, 2012, **22**, 3527–3535.
36 Y. Yao, S. Miao, S. Liu, L. P. Ma, H. Sun and S. Wang, *Chem. Eng. J.*, 2012, **184**, 326–332.
37 M. Poliakoff and P. Anastas, *Nature,* 2001, **413**, 257.
38 M. Poliakoff, J. M. Fitzpatrick, T. R. Farren and P. T. Anastas, *Science*, 2002, **297**, 807–810.
39 B. Hu, S. B. Wang, K. Wang, M. Zhang and S. H. Yu, *J. Phys. Chem. C*, 2008, **112**, 11169–11174.
40 Y. C. Lai, W. W. Yin, J. T. Liu, R. M. Xi and J. H. Zhan, *Nanoscale Res. Lett*., 2010, **5**, 302–307.
41 Z. J. Wang, H. Zhu, X. L. Wang, F. Yang and X. R. Yang, *Nanotechnology*, 2009, **20**, 465606.

42 J. R. Chiou, B. H. Lai, K. C. Hsu and D. H. Chen, *J. Hazard. Mater*., 2013, **248**, 394–400.
43 W. S. Hummers Jr. and R.E. Offeman, *J. Am. Chem. Soc.*, 1958, **80**, 1339−1339.
44 A. C. Ferrari, J. C. Meyer, V. Scardaci, C. Casiraghi, M. Lazzeri, F. Mauri, S. Piscanec, D. Jiang, K. S. Novoselov, S. Roth and A.K. Geim, *Phys. Rev. Lett*., 2006, **97**, 187401.
45 C. Stampfer, F. Molitor, D. Graf, K. Ensslin, A. Jungen, C. Hierold and L. Wirtz, *Appl. Phys. Lett.*, 2007, **91**, 241907.
46 F. Tuinstra and J. L. Koenig, *J. Chem. Phys*., 1970, **53**, 1126–1130.
47 S. Stankovich, D. A. Dikin, R. D. Piner, K. A. Kohlhaas, A. Kleinhammes, Y. Jia, Y. Wu, S. T. Nguyen and R. S. Ruoff, *Carbon*, 2007, **45**, 1558–1565.
48 C. Xu, X. Wang and J. W. Zhu, *J. Phys. Chem. C*, 2008, **112**, 19841–19845.
49 C. C. Yeh and D. H. Chen, *Appl. Catal. B: Environ*., 2014, **150–151**, 298–304.
50 A. P. Grosvenor, B. A. Kobe, M. C. Biesinger and N. S. McIntyre, *Surf. Interface Anal.*, 2004, **36**, 1564–1574.
51 Y. C. Chang and D. H. Chen, *Macromol. Biosci*., 2005, **5**, 254–261.

Table of Contents Entry

Arginine-capped iron oxide/reduced graphene oxide magnetic nano-adsorbent is synthesized via a one-step green route for acid dyes removal.